Journal of Computational Physics **160,** 126–150 (2000)
doi:10.1006/jcph.2000.6438, available online at http://www.idealibrary.com on IDEAL®

A Local Mesh Refinement Multigrid Method for 3-D Convection Problems with Strongly Variable Viscosity

Michael Albers

Institut für Geophysik, Herzberger Landstrasse 180, 37075 Göttingen, Germany
E-mail: mab@geo.physik.uni-goettingen.de

Received June 8, 1999

A numerical method for solving 3-D convection problems with variable viscosity in Cartesian geometry is presented. Equations for conservation of mass, momentum, and energy are solved using a second-order finite-volume discretization in combination with a multigrid method. Viscosity variations of 10 orders of magnitude are considered. Convergence deteriorates with increasing viscosity variations, but modifications of the multigrid algorithm are found to improve the robustness of the numerical method for very large viscosity contrasts. An efficient and flexible local mesh refinement technique is presented which is applied to various convection problems with variable viscosity. Comparisons with other numerical methods reveal that accurate results are obtained even when viscosity varies strongly.

Key Words: finite-volume discretization; multigrid methods; local mesh refinements; 3-D fluid flow; variable viscosity.

1. INTRODUCTION

On geological time scales Earth's solid mantle can be considered as a highly viscous fluid. The creeping flow is predominantly thermally driven by heat from Earth's core and radioactive heat release in the mantle [1]. Mantle viscosity is of the order 10^{21} Pa s, but it can vary by several orders of magnitude due to the strong temperature and pressure dependence [2]. Geodynamical modeling of convection in Earth's or in other planetary mantles is simplified because inertia and Coriolis forces can be neglected. On the other hand, the extreme variability of viscosity complicates the numerical solution. Despite its well-known influence on convection patterns variable viscosity has often been ignored or restricted in 3-D convection models because of limited computer resources. Therefore, the development of fast numerical methods which can handle strongly variable viscosity is important for geodynamical modeling.

0019-9991/00 $35.00

A very efficient numerical method for solving elliptic differential equations is multigrid iteration. The basic idea of multigrid is to approximate and reduce the long-wavelength error of the solution, which converges very slowly on grids with large numbers of grid points, on coarser grids with successively decreasing numbers of grid points. By doing multigrid iterations convergence rates can be obtained which are independent of the problem size. A detailed description of the various multigrid schemes can be found, for example, in [3–6].

The multigrid concept has been applied successfully to a wide range of problems, including calculation of fluid flow. Various multigrid methods for solving Stokes and Navier–Stokes equations with constant viscosity have been presented, for example in [4, 7–10]. Parmentier *et al.* [11] have used a multigrid solver in a 3-D convection model for isoviscous fluid flow in Cartesian geometry. By using the streamfunction formulation they have been able to reduce Stokes equations to a pair of Poisson equations which are solved by multigrid iterations. While much work has been spent on multigrid solutions of isoviscous fluid flow, only few papers deal with variable viscosity. Baumgardner [12] has presented a multigrid method for solving convection problems in 3-D spherical geometry. This method has been used in calculations with constant viscosity [12] as well as with depth-dependent viscosity [13, 14] and with 3-D varying viscosity [15]. Moresi and Solomatov [16] have presented a multigrid method for convection problems with variable viscosity in Cartesian geometry which has been used in 2-D and in 3-D calculations [16–18]. Stokes equations are solved by an Uzawa iteration scheme. Iteration for velocity is carried out by a multigrid method, while a conjugate gradient scheme is used for pressure iteration. Both multigrid methods are based on a finite-element discretization. Tackley [19] has developed a multigrid method for 3-D convection problems with variable viscosity in Cartesian geometry using a finite-volume discretization. This method has been applied successfully to a variety of convection problems, e.g., [20–22], including calculations with extremely variable viscosity [23]. Trompert and Hansen [24] have presented a different multigrid method, though they have used a similar discretization scheme. By modifying the multigrid smoother they have been able to treat viscosity variations up to 10^9, but convergence of the multigrid method becomes slow if viscosity varies strongly. Auth and Harder [25] have investigated multigrid solutions of convection problems with strongly varying viscosity in 2-D. They have increased the stability of the multigrid method by using more complex multigrid cycles that require only a slightly larger computational effort.

I solve 3-D convection problems with variable viscosity in Cartesian geometry, following the approaches given by Tackley [19] and Trompert and Hansen [24]. I have improved these approaches by the implementation of a different multigrid scheme which can handle local grid refinements. In typical convection problems the solution varies rapidly in some parts of the model domain, e.g., in boundary layers or near stagnation points, while it changes more smoothly in most other regions. This suggests to use a nonuniform numerical grid to achieve good resolution where needed at moderate overall costs. In the context of standard finite-difference or finite-volume techniques, uneven mesh spacing leads to more complex difference equations and is therefore often avoided. The use of a multigrid iteration scheme allows the implementation of a more efficient technique for creating local mesh refinements. Such a technique is described here and is tested both for published benchmarks and for particular problems in which large local gradients in all variables play an essential role.

2. GOVERNING EQUATIONS

I examine thermally driven convection in a highly viscous, incompressible fluid with infinite Prandtl number in a 3-D Cartesian domain. The Boussinesq approximation is adopted. The time-dependent fluid flow is described by the following nondimensional equations derived from the conservation laws of mass, momentum, and energy, respectively,

$$\nabla \cdot \mathbf{v} = 0, \tag{1}$$

$$-\nabla p + \nabla \cdot (\eta(\nabla \mathbf{v} + (\nabla \mathbf{v})^T)) + \mathrm{Ra} T \mathbf{e}_z = 0, \tag{2}$$

$$\frac{\partial T}{\partial t} + \nabla \cdot (\mathbf{v} T) = \nabla^2 T. \tag{3}$$

$\mathbf{v} = (u, v, w)$ means velocity, p is the nonhydrostatic pressure component, η dynamic viscosity, T temperature, $\boldsymbol{e}_z$ unit vector antiparallel to the direction of gravity, and t time.

Equations (1)–(3) contain only one dimensionless parameter, the Rayleigh number Ra, which is defined by

$$\mathrm{Ra} = \frac{\rho_0 \alpha g \Delta T h^3}{\kappa \eta_0},$$

with α thermal expansivity, g gravitational acceleration, ΔT temperature drop across the box, h height of the box, κ thermal diffusivity, and ρ_0 and η_0 reference values of density and viscosity, respectively. The equations are scaled with h (length), h^2/κ (time), ΔT (temperature), and $\eta_0 \kappa / h^2$ (pressure).

Viscosity depends on temperature and depth. The variability of the nondimensional viscosity is described by Arrhenius law,

$$\eta = A \exp\left(\frac{E_1 + E_2(1 - z)}{T + E_3}\right), \tag{4a}$$

or by a temperature-dependence of the form

$$\eta = \exp(-E_4 T), \tag{4b}$$

with parameters E_1–E_4 controlling the temperature and depth dependence and A defining the reference value of viscosity.

3. NUMERICAL METHOD

3.1. *Finite-Volume Discretization*

The model domain is divided into uniform cells Ω_{ijk} with i, j, k being indices in x-, y-, and z-direction, respectively. A staggered grid is used. Temperature and pressure are located at the center of the grid cells the velocity components at the center of the cell faces normal to the direction of the velocity components (Fig. 1).

This staggered grid was first introduced by Harlow and Welch [26] and afterward used in most of the numerical methods based on the primitive variable formulation, e.g., [7, 19, 24, 25, 27]. By this kind of discretization artificial pressure and velocity oscillations are avoided [28] and greater accuracy than on nonstaggered grids is obtained [29].

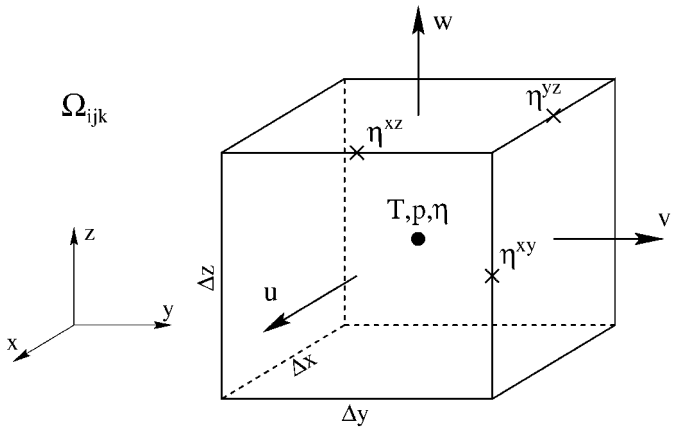

FIG. 1. Staggered grid location of variables in grid cell Ω_{ijk}.

Equations (1)–(3) are discretized using a second-order control-volume method. The model domain is divided into control volumes which must not necessarily correspond to the grid cells. The equations are integrated over these volumes. The discretized equations are obtained by approximating the required integrals by the grid point values. The most attractive feature of the control-volume formulation is that the resulting solution satisfies the conservation of mass, momentum, and energy exactly over the control volume, independent of the number of grid points. A detailed description of the control-volume discretization of the governing equations on a staggered grid can be found, for example, in [6, 28].

The continuity Eq. (1) is integrated over control volumes that match with the grid cells, yielding

$$\frac{u_{ijk} - u_{i-1jk}}{\Delta x} + \frac{v_{ijk} - v_{ij-1k}}{\Delta y} + \frac{w_{ijk} - w_{ijk-1}}{\Delta z} = 0, \tag{5}$$

with Δx, Δy, and Δz grid spacing in x-, y-, and z-direction, respectively.

The control volumes of the momentum Eq. (2) are staggered in the same way as velocity, resulting in the following set of discretized equations,

$$-\frac{p_{i+1jk} - p_{ijk}}{\Delta x} + \frac{\tau^{xx}_{i+1jk} - \tau^{xx}_{ijk}}{\Delta x} + \frac{\tau^{xy}_{ijk} - \tau^{xy}_{ij-1k}}{\Delta y} + \frac{\tau^{xz}_{ijk} - \tau^{xz}_{ijk-1}}{\Delta z} = 0, \tag{6a}$$

$$-\frac{p_{ij+1k} - p_{ijk}}{\Delta y} + \frac{\tau^{xy}_{ijk} - \tau^{xy}_{i-1jk}}{\Delta x} + \frac{\tau^{yy}_{ij+1k} - \tau^{yy}_{ijk}}{\Delta y} + \frac{\tau^{yz}_{ijk} - \tau^{yz}_{ijk-1}}{\Delta z} = 0, \tag{6b}$$

$$-\frac{p_{ijk+1} - p_{ijk}}{\Delta z} + \frac{\tau^{xz}_{ijk} - \tau^{xz}_{i-1jk}}{\Delta x} + \frac{\tau^{yz}_{ijk} - \tau^{yz}_{ij-1k}}{\Delta y} + \frac{\tau^{zz}_{ijk+1} - \tau^{zz}_{ijk}}{\Delta z} = -\mathrm{Ra}\frac{T_{ijk+1} + T_{ijk}}{2}, \tag{6c}$$

with

$$\tau^{xx}_{ijk} = 2\eta_{ijk}\frac{u_{ijk} - u_{i-1jk}}{\Delta x},$$

$$\tau^{yy}_{ijk} = 2\eta_{ijk}\frac{v_{ijk} - v_{ij-1k}}{\Delta y},$$

$$\tau_{ijk}^{zz} = 2\eta_{ijk}\frac{w_{ijk} - w_{ijk-1}}{\Delta z},$$
$$\tau_{ijk}^{xy} = \eta_{ijk}^{xy}\left(\frac{u_{ij+1k} - u_{ijk}}{\Delta y} + \frac{v_{i+1jk} - v_{ijk}}{\Delta x}\right),$$
$$\tau_{ijk}^{xz} = \eta_{ijk}^{xz}\left(\frac{u_{ijk+1} - u_{ijk}}{\Delta z} + \frac{w_{i+1jk} - w_{ijk}}{\Delta x}\right),$$
$$\tau_{ijk}^{yz} = \eta_{ijk}^{yz}\left(\frac{v_{ijk+1} - v_{ijk}}{\Delta z} + \frac{w_{ij+1k} - w_{ijk}}{\Delta y}\right).$$

The viscosity η_{ijk} is defined at the center of the grid cells. It is calculated from temperature and depth using (4a) or (4b). Additional viscosity values η_{ijk}^{xy}, η_{ijk}^{xz}, η_{ijk}^{yz} at the midpoints of cell edges (Fig. 1) are interpolated from the four surrounding cell-centered viscosities. Following the general approach of discretizing equations with discontinuous coefficients given by Wesseling [6, 30], a method based on continuity of stress at cell faces has to be used, if viscosity differs strongly between adjacent cells. Continuity of stress can be satisfied by using harmonic interpolation for viscosity at cell edges. This kind of interpolation has been used by Ogawa *et al.* [27]. However, in the method presented here harmonic interpolation does not lead to more accurate results than bilinear interpolation. Therefore, the simpler bilinear interpolation has been used.

The energy Eq. (3) is discretized in time using a finite-difference method with implicit treatment of the advection and diffusion terms,

$$\frac{T^{n+1} - T^n}{\Delta t} = \Theta(\nabla^2 T^{n+1} - \nabla(\mathbf{v}T)^{n+1}) + (1 - \Theta)(\nabla^2 T^n - \nabla(\mathbf{v}T)^n), \tag{7}$$

where Δt is the time step size and the superscripts n and $n+1$ denote values at old and new time, respectively. While the explicit scheme ($\Theta = 0$) is stable only for small time steps, schemes with $\Theta \geq 0.5$ are unconditionally stable. The fully implicit backward Euler scheme ($\Theta = 1$) with large time steps is used for calculating steady-state solutions. For time-dependent fluid flow the second-order accurate implicit Crank–Nicolson scheme ($\Theta = 0.5$) is used with a time step size limited by the Courant criterion,

$$\Delta t < \min\left(\frac{|u|}{\Delta x} + \frac{|v|}{\Delta y} + \frac{|w|}{\Delta z}\right)^{-1}.$$

Although the time-stepping scheme is unconditionally stable the Courant condition has been applied to time-dependent solutions in order to achieve good resolution in time.

For the spatial discretization I have integrated (7) over the grid cell volume. Afterward the discretized continuity Eq. (5) multiplied by the temperature is subtracted to avoid numerical instabilities [28], yielding

$$T_{ijk}^{n+1} + \Theta\Delta t J_{ijk}^{n+1} = T_{ijk}^n - (1 - \Theta)\Delta t J_{ijk}^n, \tag{8}$$

with

$$J_{ijk} = \frac{J_{i+\frac{1}{2}jk}^x - J_{i-\frac{1}{2}jk}^x}{\Delta x} + \frac{J_{ij+\frac{1}{2}k}^y - J_{ij-\frac{1}{2}k}^y}{\Delta y} + \frac{J_{ijk+\frac{1}{2}}^z - J_{ijk-\frac{1}{2}}^z}{\Delta z},$$

and

$$J^x_{i+\frac{1}{2}jk} = (uT)_{i+\frac{1}{2}jk} - \frac{T_{i+1jk} - T_{ijk}}{\Delta x} - u_{ijk}T_{ijk},$$
$$J^y_{ij+\frac{1}{2}k} = (vT)_{ij+\frac{1}{2}k} - \frac{T_{ij+1k} - T_{ijk}}{\Delta y} - u_{ijk}T_{ijk},$$
$$J^z_{ijk+\frac{1}{2}} = (wT)_{ijk+\frac{1}{2}} - \frac{T_{ijk+1} - T_{ijk}}{\Delta z} - w_{ijk}T_{ijk}.$$

The diffusion term is approximated by central differences while an upwind scheme is used for the advection term. Two different schemes have been implemented, namely the upwind-biased Fromm scheme used by Trompert and Hansen [24] and the power-law scheme given by Patankar [28]. The advective heat flux in x-direction uT at cell boundary $(i+\frac{1}{2}, j, k)$ is given in the Fromm scheme by

$$(uT)_{i+\frac{1}{2}jk} = \max(u_{ijk}, 0)\left(T_{ijk} + \frac{1}{4}(T_{i+1jk} - T_{i-1jk})\right) + \min(u_{ijk}, 0)\left(T_{i+1jk} - \frac{1}{4}(T_{i+2jk} - T_{ijk})\right), \tag{9}$$

and in the power-law scheme by

$$(uT)_{i+\frac{1}{2}jk} = \left(\max(u_{ijk}, 0) + \frac{\max((1 - 0.1\cdot|\mathrm{Pe}_{ijk}|)^5, 0) - 1}{\Delta x}\right)T_{ijk} + \left(\min(u_{ijk}, 0) - \frac{\max((1 - 0.1\cdot|\mathrm{Pe}_{ijk}|)^5, 0) - 1}{\Delta x}\right)T_{i+1jk}, \tag{10}$$

and similarly at other cell boundaries. $\mathrm{Pe}_{ijk} = u_{ijk}\Delta x$ is the local grid Peclet number. For large Peclet numbers ($|\mathrm{Pe}_{ijk}| \geq 10$) the power-law scheme reduces to the first-order upwind scheme with neglected diffusion term. For small Peclet numbers it comes closer to the central scheme [28].

In the following the discretized equations (5), (6a)–(6c), and (8) are formally written as matrix equation

$$\begin{pmatrix} A(\eta(T)) & G & B \\ D & 0 & 0 \\ 0 & 0 & C(\mathbf{v}) \end{pmatrix} \begin{pmatrix} \mathbf{v} \\ p \\ T \end{pmatrix} = \begin{pmatrix} \mathbf{f} \\ f_4 \\ f_5 \end{pmatrix}. \tag{11}$$

Nonlinearities occur in the advection term of the energy equation and in the viscous force term of the momentum equation due to the temperature-dependence of viscosity.

3.2. *Multigrid Method*

The discretized Eqs. (11) are solved using a multigrid method. In contrast to most of the previous multigrid methods I use the full-approximation-storage (FAS) algorithm [3, 4] in which the full solution is calculated at all grid levels. Fine and coarser grids differ only in the way of calculating the right-hand-side of (11). This is different from other multigrid algorithms which calculate residuals and corrections instead of the full solution at coarser

grids. The algorithm starts at the finest grid and visits all coarser grids in the order given by the multigrid cycle. A standard cell-centered coarsening is applied meaning that one coarse grid cell includes eight fine grid cells. Although the implemented algorithm is suitable for nonlinear differential equations, I have linearized (11). The matrices $A(\eta(T))$ and $C(\mathbf{v})$ in (11) are computed on all grids in advance using the values of T and $\mathbf{v}$ obtained in the previous multigrid cycle. At the end of each multigrid cycle they are recomputed.

Two different strategies for solving (11) have been implemented. The first one solves all equations in a coupled manner yielding second-order accuracy both in space and time. In the second one the energy equation is decoupled from the continuity and momentum equations by using the velocity at old time in the advection term. The temperature at new time is calculated first. Afterward new velocity and pressure are computed from the temperature. This strategy reduces the accuracy to first order in time, but it is computationally cheaper than the coupled solution and more robust when large time steps are used. Therefore, it is prefered for calculating steady-state solutions, whereas the coupled solution strategy is used for time-dependent calculations.

3.2.1. Smoother. Because of the occurrence of a zero block on the main diagonal in (11), basic iterative methods like Jacobi or Gauss–Seidel which make use of the inverse of the main diagonal, cannot be applied as smoother. Smoothing methods of the distributive iteration type are necessary. I have implemented the SIMPLER (semi implicit method for pressure-linked equations revised) algorithm by Patankar [28], because with slight modifications its suitability for calculations with strongly variable viscosity has been shown [24, 31].

The SIMPLER method can be split in following parts:

1. Calculation of new temperature using energy equation.
2. Calculation of new pressure using

$$-DS^{-1}Gp = f_4 - D(\mathbf{v} + S^{-1}(f - BT - A\mathbf{v})), \tag{12}$$

with S diagonal of matrix A. This pressure equation is obtained by combining momentum and continuity equations.

3. Calculation of new velocity using momentum equation.
4. Calculation of a pressure correction δp using

$$-DS^{-1}G\delta p = f_4 - D\mathbf{v}. \tag{13}$$

5. Correction of velocity by adding $-S^{-1}G\delta p$ to fulfill continuity equation.

In the case of a decoupled solution strategy step 1 is left out and new temperature is calculated in separate multigrid cycles.

The calculations in steps 1–4 are carried out by single pointwise Gauß–Seidel iterations. If the Fromm scheme is used for the advective heat flux, matrix C is not diagonally dominant and basic iterative methods are not applicable. The defect-correction iteration [32] has been applied. Instead of solving $CT = f_5$ the defect-correction equation

$$\tilde{C}T = f_5 - (C - \tilde{C})\,T, \tag{14}$$

with $\tilde{C}$ containing the first-order upwind scheme for advection is solved. The right-hand side is recomputed after each multigrid cycle. Because $\tilde{C}$ is diagonally dominant pointwise Gauß–Seidel iteration is applicable to (14).

3.2.2. Prolongation and restriction. In multigrid methods data have to be transfered from fine to coarse grids (restriction) and from coarse to fine grids (prolongation). In order to obtain a mesh size independent rate of convergence the prolongation and restriction operators have to satisfy

$$m_{\mathrm{P}} + m_{\mathrm{R}} > 2m, \tag{15}$$

where m_{P} and m_{R} are defined as the orders of interpolation plus one used for prolongation and restriction and $2m$ is the order of the partial differential equation to be solved [5, 6, 33].

I use linear interpolation for prolongation. Temperature and pressure of the fine grid are expressed by Taylor series expansions around the coarse grid points up to first-order terms, e.g.,

$$\begin{aligned}
T_{2i2j2k} &= \bar{T}_{ijk} + T_x + T_y + T_z,\\
T_{2i-12j2k} &= \bar{T}_{ijk} - T_x + T_y + T_z,\\
T_{2i2j-12k} &= \bar{T}_{ijk} + T_x - T_y + T_z,\\
&\vdots\\
T_{2i-12j-12k-1} &= \bar{T}_{ijk} - T_x - T_y - T_z,
\end{aligned}$$

with

$$\begin{aligned}
T_x &= \frac{\bar{T}_{i+1jk} - \bar{T}_{i-1jk}}{8},\\
T_y &= \frac{\bar{T}_{ij+1k} - \bar{T}_{ij-1k}}{8},\\
T_z &= \frac{\bar{T}_{ijk+1} - \bar{T}_{ijk-1}}{8},
\end{aligned}$$

and similarly for pressure. Overbars denote coarse grid values. Because velocity is defined at the center of cell faces modified prolongation operators have to be used. For velocity components of the fine grid that belong to coarse grid cell faces Taylor series expansions in the directions perpendicular to the velocity components are applied, e.g.,

$$\begin{aligned}
u_{2i2j2k} &= \bar{u}_{ijk} + u_y + u_z,\\
u_{2i2j-12k} &= \bar{u}_{ijk} - u_y + u_z,\\
u_{2i2j2k-1} &= \bar{u}_{ijk} + u_y - u_z,\\
u_{2i2j-12k-1} &= \bar{u}_{ijk} - u_y - u_z,
\end{aligned}$$

with

$$\begin{aligned}
u_y &= \frac{\bar{u}_{ij+1k} - \bar{u}_{ij-1k}}{8},\\
u_z &= \frac{\bar{u}_{ijk+1} - \bar{u}_{ijk-1}}{8}.
\end{aligned}$$

Afterward the velocity components at intermediate fine grid cell faces are interpolated from the fine grid values belonging to coarse grid cell faces, e.g.,

$$u_{2i-12j2k} = \frac{u_{2i2j2k} + u_{2i-22j2k}}{2},$$
$$u_{2i-12j-12k} = \frac{u_{2i2j-12k} + u_{2i-22j-12k}}{2},$$
$$u_{2i-12j2k-1} = \frac{u_{2i2j2k-1} + u_{2i-22j2k-1}}{2},$$
$$u_{2i-12j-12k-1} = \frac{u_{2i2j-12k-1} + u_{2i-22j-12k-1}}{2}.$$

The prolongation operators for the other velocity components are obtained in a similar way.

For restriction the coarse grid values of temperature and pressure are computed by averaging the fine grid values of the eight corresponding fine grid cells, e.g.,

$$\bar{T}_{ijk} = \frac{T_{2i2j2k} + T_{2i-12j2k} + T_{2i2j-12k} + \cdots + T_{2i-12j-12k-1}}{8},$$

and similarly for pressure. For velocity the fine grid values are weighted in the direction of the velocity component by using the inverse of linear interpolation and are averaged in perpendicular directions, e.g.,

$$\bar{u}_{ijk} = \frac{\tilde{u}_{2i-1jk} + 2\tilde{u}_{2ijk} + \tilde{u}_{2i+1jk}}{4},$$

with

$$\tilde{u}_{2ijk} = \frac{u_{2i2j2k} + u_{2i2j-12k} + u_{2i2j2k-1} + u_{2i2j-12k-1}}{4},$$

and similarly for other velocity components.

In problems with discontinuous coefficients standard transfer operators are sufficient for cell-centered discretization, but for vertex-centered discretization operator-dependent prolongation and restriction operators have to be used [6, 30, 34]. In the staggered grid formulation a vertex-centered discretization is applied for velocity components in the direction of the velocity components. Following the approach given by Alcouffe *et al.* [35] I have used prolongation and restriction operators, which fulfill the continuity of stress at intermediate cell faces. No significant differences have been found between standard and operator-dependent transfer operators. Therefore, the prolongation and restriction operators described above have been finally implemented.

The residuals of (11) also have to be transfered to coarser grids. The same restriction operators have been used for variables and residuals. With these operators for prolongation and restriction I obtain $m_P = 2$ and $m_R = 1$ and satisfy condition (15) for second-order differential equations.

3.2.3. Coarse grid approximation. In multigrid methods the fine grid Eq. (11) has to be approximated by coarse grid equations. There are basically two different ways of calculating the coarse grid matrices. In the discretization coarse grid approximation [6] the coarse grid matrices are obtained in the same way as the fine grid matrix by discretizing the differential equation. Therefore, the coarse grid approximation is straightforward, but it can

be insufficient on very coarse grids if the differential equation contains strongly variable coefficients. In the Galerkin coarse grid approximation [6] the coarse grid matrix $\bar{M}$ is calculated from the fine grid matrix M by

$$\bar{M} = RMP,$$

with R and P restriction and prolongation operators. The stencil of the coarse grid matrix depends on the choice of restriction and prolongation operators. In order to avoid that most of the computational work which is saved by doing calculations on coarser grids with less grid points is consumed by more complicated coarse grid matrices, it is essential to use restriction and prolongation operators that increase the stencil of the coarse grid matrices as little as possible. Such transfer operators for the 2-D Navier–Stokes equations have been presented by Zeng and Wesseling [10]. The Galerkin coarse grid approximation is often used for differential equations with discontinuous coefficients, for example in [10, 30, 34–37].

Because of simplicity I have implemented the discretization coarse grid approximation. In order to calculate the coarse grid matrices the viscosity has to be known on coarser grids. I use restriction of viscosity from finer grids. The viscosity at the center of the coarse grid cell is computed by averaging the cell-centered viscosities of the eight corresponding fine grid cells,

$$\bar{\eta}_{ijk} = \frac{\eta_{2i2j2k} + \eta_{2i-12j2k} + \eta_{2i2j-12k} + \cdots + \eta_{2i-12j-12k-1}}{8}. \tag{16a}$$

Other viscosities are transferred to coarser grids by using the inverse of bilinear interpolation, yielding

$$\begin{aligned}
\bar{\eta}^{xy}_{ijk} = {} & \frac{\tilde{\eta}^{xy}_{2i-12j-12k} + 2\tilde{\eta}^{xy}_{2i2j-12k} + \tilde{\eta}^{xy}_{2i+12j-12k}}{16} \\
& + \frac{2\tilde{\eta}^{xy}_{2i-12j2k} + 4\tilde{\eta}^{xy}_{2i2j2k} + 2\tilde{\eta}^{xy}_{2i+12j2k}}{16} \\
& + \frac{\tilde{\eta}^{xy}_{2i-12j+12k} + 2\tilde{\eta}^{xy}_{2i2j+12k} + \tilde{\eta}^{xy}_{2i+12j+12k}}{16},
\end{aligned} \tag{16b}$$

$$\begin{aligned}
\bar{\eta}^{xz}_{ijk} = {} & \frac{\tilde{\eta}^{xz}_{2i-12j2k-1} + 2\tilde{\eta}^{xz}_{2i2j2k-1} + \tilde{\eta}^{xz}_{2i+12j2k-1}}{16} \\
& + \frac{2\tilde{\eta}^{xz}_{2i-12j2k} + 4\tilde{\eta}^{xz}_{2i2j2k} + 2\tilde{\eta}^{xz}_{2i+12j2k}}{16} \\
& + \frac{\tilde{\eta}^{xz}_{2i-12j2k+1} + 2\tilde{\eta}^{xz}_{2i2j2k+1} + \tilde{\eta}^{xz}_{2i+12j2k+1}}{16},
\end{aligned} \tag{16c}$$

$$\begin{aligned}
\bar{\eta}^{yz}_{ijk} = {} & \frac{\tilde{\eta}^{yz}_{2i2j-12k-1} + 2\tilde{\eta}^{yz}_{2i2j2k-1} + \tilde{\eta}^{yz}_{2i2j+12k-1}}{16} \\
& + \frac{2\tilde{\eta}^{yz}_{2i2j-12k} + 4\tilde{\eta}^{yz}_{2i2j2k} + 2\tilde{\eta}^{yz}_{2i2j+12k}}{16} \\
& + \frac{\tilde{\eta}^{yz}_{2i2j-12k+1} + 2\tilde{\eta}^{yz}_{2i2j2k+1} + \tilde{\eta}^{yz}_{2i2j+12k+1}}{16},
\end{aligned} \tag{16d}$$

with

$$\tilde{\eta}^{xy}_{2i2j2k} = \frac{\eta^{xy}_{2i2j2k} + \eta^{xy}_{2i2j2k-1}}{2},$$
$$\tilde{\eta}^{xz}_{2i2j2k} = \frac{\eta^{xz}_{2i2j2k} + \eta^{xz}_{2i2j-12k}}{2},$$
$$\tilde{\eta}^{yz}_{2i2j2k} = \frac{\eta^{yz}_{2i2j2k} + \eta^{yz}_{2i-12j2k}}{2}.$$

3.3. *Local Mesh Refinements*

Multigrid methods offer a very efficient and flexible technique for creating local mesh refinements. The nonuniform grid is generated by the same set of uniform subgrids which are used in the multigrid method. Local mesh refinements are introduced by some of the finest grids covering only parts of the model domain. A 2-D example is shown in Fig. 2. Because the iteration process of the multigrid method takes places on uniform grids the discretization scheme does not have to be changed if grid refinements are introduced. The difference equations which have to be solved remain as simple as in the case without grid

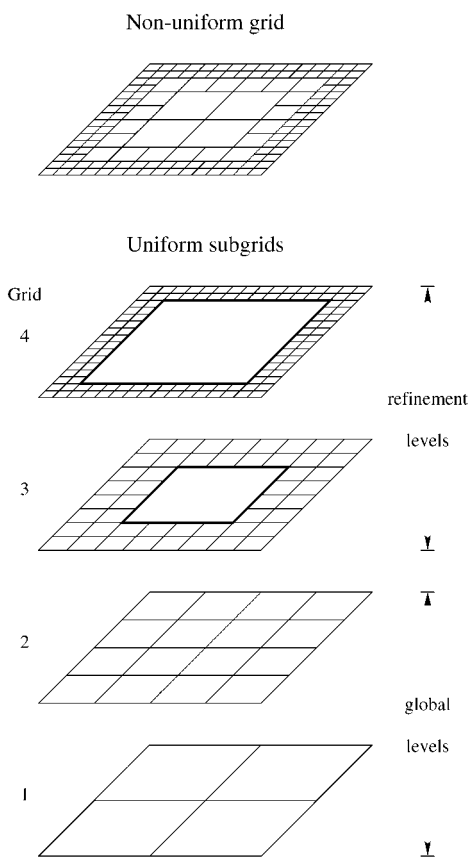

FIG. 2. Generation of a nonuniform grid by a set of uniform subgrids (2-D example). On refinement levels grids cover only parts of the model domain. Thick lines represent interior grid boundaries that are not boundaries of the model domain.

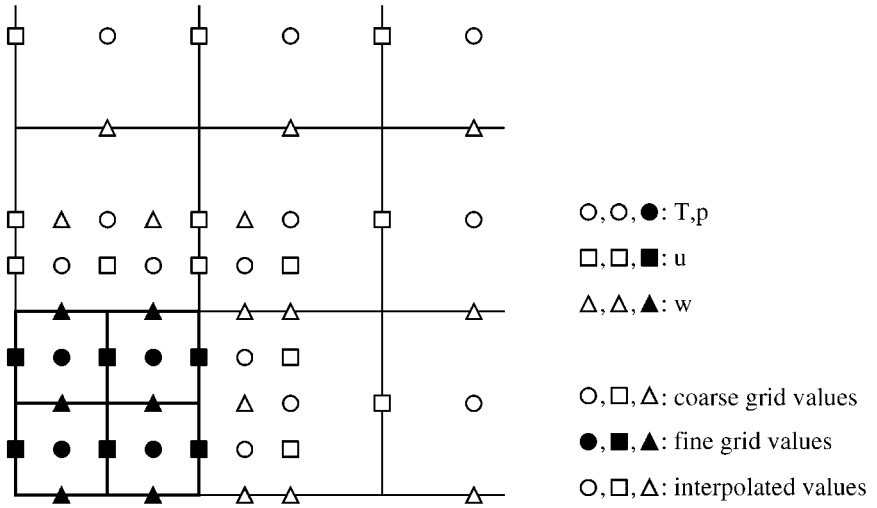

FIG. 3. Location of variables on a nonuniform staggered grid (2-D example). At interior boundaries of the grid refinement variables are interpolated from the coarse grid.

refinements. The only modification occurs in the calculation of the right-hand side. It has to be taken into account that a coarse-grid correction is calculated in regions where finer grids exist, while in other parts of the model domain the grid acts as the finest grid. It is compatible with the FAS-algorithm to have different finest grids in different regions because the full solution is treated at all grid levels, whereas there is a conflict in other multigrid algorithms in having correction of the fine grid solution in some regions and full solution in others. A detailed description of this mesh refinement method can be found, for example, in [3, 38].

On refinement levels (levels on which grids do not extend over the whole model domain) grids contain interior boundaries that are not boundaries of the model domain (thick lines in Fig. 2). Therefore, no boundary conditions can be applied. In order to define the difference equations at these boundaries values for temperature, pressure, and velocity are interpolated from the next coarser grid. Figure 3 shows the staggered grid locations of the interpolated values. The accuracy of the numerical solution depends on the order of this interpolation. The error introduced by the interpolation should be not larger than the local truncation error which is of order $m + p$ with m order of the differential equation and p approximation order [38]. In this case with $m = p = 2$ the interpolation should be at least of fourth order. Therefore, cubic interpolation for calculating values at interior boundaries have been implemented.

By using this refinement method the number of grid points does not necessarily decrease on coarser grids. Multigrid cycles that use coarser grids more than once during each cycle, e.g., F or W cycles, do not provide a linear dependence of computational work on number of grid points. A modified algorithm based on a work-to-accuracy exchange rate has been developed by Bai and Brandt [38], which obtains the usual multigrid efficiency. I have implemented a simpler approach using modified multigrid cycles. On global grid levels all usual multigrid cycles are allowed, but on refinement levels they are always changed to V cycles. V cycles visit coarser grids only once during each cycle. This modification minimizes the increase of computational work due to local mesh refinements.

4. RESULTS

4.1. *Convergence Tests*

In previous investigations convergence problems of the multigrid method have been reported if viscosity varies strongly [19, 24, 25]. In this section different variants of the multigrid method have been tested. Their convergence behavior in calculations with large viscosity variations has been determined, in order to find the best implementation for geodynamical convection problems.

Convergence tests have been done by solving Stokes equations only for a prescribed temperature field. Temperature has been taken from a 3-D time-dependent calculation in a box with $64 \times 64 \times 64$ equally spaced grid cells. Temperature is fixed to zero at the top and to one at the bottom. Reflecting symmetry is assumed at the sidewall, zero shear stress at all boundaries. Viscosity depends on temperature according to (4b) with $E_4 = \ln(10^5)$. The Rayleigh number is $\mathrm{Ra} = 1000$ based on viscosity $\eta(T = 0)$. The calculation has been started from a conductive temperature distribution to which small-scale perturbations have been added.

Three different temperature fields have been used in the convergence tests. Temperature 1 (Fig. 4, top) is taken from an early stage of the time evolution, with diapiric thermal plumes rising from an unstable bottom boundary layer. Temperature 2 (Fig. 4, middle) belongs to a transient stage during time evolution when the flow structure is reorganized. Temperature 3 (Fig. 4, bottom) shows two major upwellings beneath a top boundary layer which covers most of the temperature drop across the box. These temperature fields have been chosen because they provide a different distribution of local viscosity gradients. In temperature 1 viscosity varies strongly in the bottom boundary layer and in the rising plume heads. Because of the complicated structure of temperature 2, local viscosity gradients occur throughout the box, but they are not as large as in temperature 1. In temperature 3 the interior of the box is nearly isoviscous and most of the global viscosity contrast is covered by the top boundary layer.

Although temperature has been prescribed in the convergence tests the viscosity contrast has been varied by changing the temperature-dependence of viscosity. The convergence behavior of different multigrid variants is shown in Fig. 5. The number of multigrid cycles which are required for reducing the initial L^2-norm of the residual by eight orders of magnitude is presented as a function of the global viscosity contrast. V, F, and W cycles have been used with two pre- and postsmoothers. In addition, modifications of the V and W cycles have been tested. In the modified W cycle the number of pre- and postsmoothers have been increased by a factor of 2 from one grid to the next coarser grid. In the modified V cycle they have been successively increased by a factor of 4, leading to the same total number of smoothing iterations on coarser grids in the modified V and W cycles. F, W, and the modified V and W cycles are approximately 15, 20, and 50% more expensive, respectively, than V cycles.

The convergence rates deteriorate with the increasing variability of viscosity for all multigrid variants. Above a certain viscosity contrast the numerical method diverges. The multigrid method becomes more stable if more complex multigrid cycles instead of the most simple V cycle are used, in agreement with results obtained in 2-D [25]. Comparison of modified V and W cycles reveal that this improvement is not caused by the order in which the coarser grids are visited but by the total number of smoothing iterations on coarser grids.

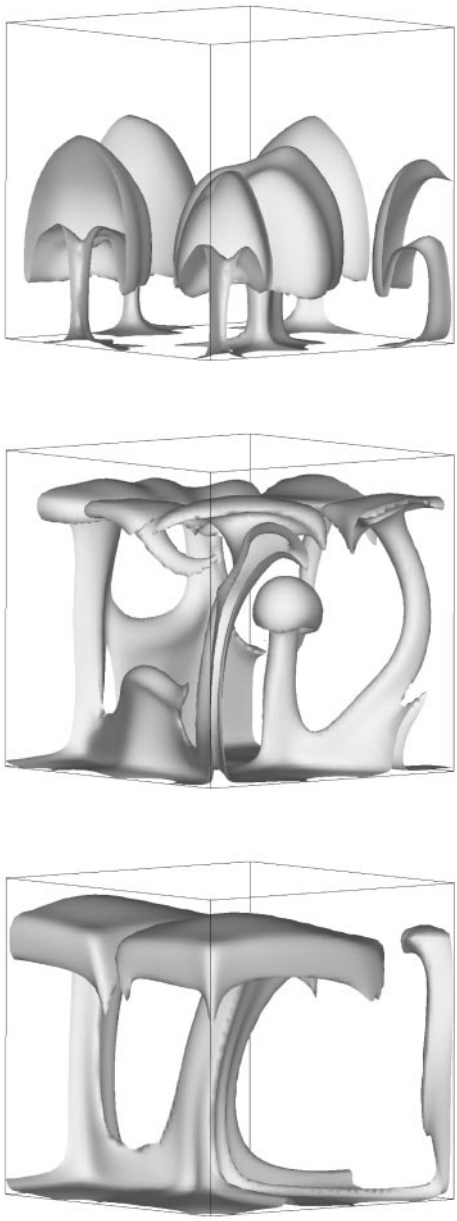

FIG. 4. Temperature fields of a 3-D time dependent calculation with variable viscosity at $t \approx 0.0004$ (top, isosurface $T = 0.85$), $t \approx 0.032$ (middle, isosurface $T = 0.88$), and $t \approx 0.060$ (bottom, isosurface $T = 0.90$).

If the number of iterations at each level is equalized the robustness of V and W cycles is similar.

Convergence rates of the modified V and W cycles are acceptable for global viscosity variations up to 10^8 for temperature 1 (Fig. 5, top) which is equivalent to local viscosity contrasts of 24,000 over one grid cell in the bottom boundary layer. For temperatures 2 and 3 global viscosity variations of 10^{10} and 10^9, respectively, have been reached (Fig. 5, middle and bottom, respectively). However, these larger global viscosity variations belong to local viscosity contrasts of 1700 and 700 over one grid cell which are much smaller than the

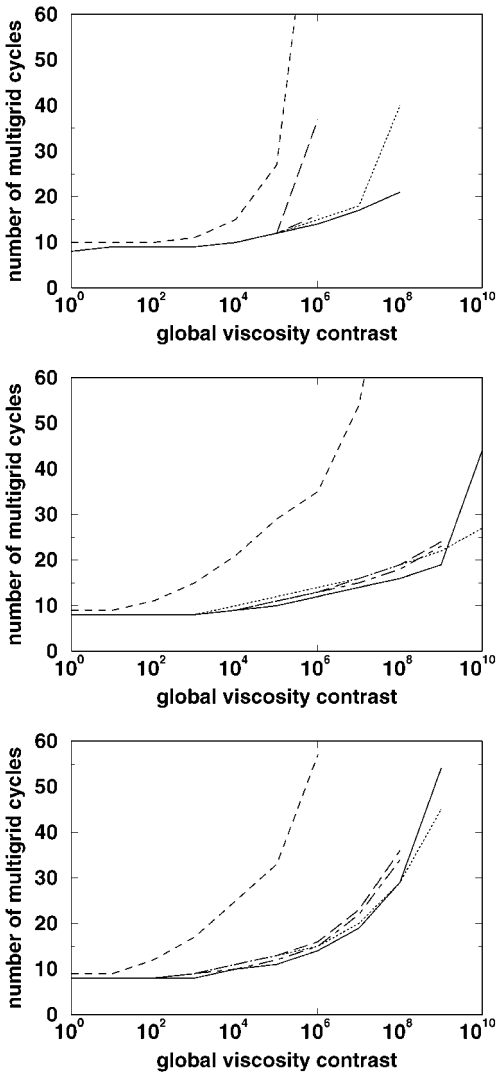

FIG. 5. Multigrid convergence for temperature fields given in Fig. 4: temperature 1 (top), temperature 2 (middle), and temperature 3 (bottom). V cycles (dashed), F cycles (long dashed), W cycles (dot-dashed), modified V cycles (dotted), and modified W cycles (solid) are used. The curves end when divergence of the multigrid method occurs.

local viscosity contrast that has been obtained for temperature 1. This indicates that neither the global viscosity variations nor the local viscosity contrasts by themselves control the convergence behavior of the multigrid method. It seems that the volumetrical distribution of viscosity variations is just as important.

The robustness of the multigrid method is extremely sensitive to the kind of viscosity calculation on coarser grids if viscosity varies strongly. I have used different methods, including direct calculation from the functional dependence on temperature and depth and restriction from finer grids. It turned out that calculation of viscosity directly from temperature and depth on coarser grids is not suitable, consistent with 2-D results [25]. Various restriction operators, including the viscosity restriction presented by Trompert and Hansen [24], yield good convergence rates for some temperature distributions but not for others.

The viscosity restriction (16a)–(16d) that was finally implemented has produced on average the best results for all temperature distributions.

The convergence tests show that acceptable convergence rates of the multigrid method are obtained for global viscosity variations up to at least eight orders of magnitude. Calculations with even larger viscosity variations have been done by increasing the number of pre- and postsmoothers in the multigrid algorithm. An alternative way for making multigrid methods more stable has been presented by Trompert and Hansen [24]. They have found that convergence problems can be reduced by solving the pressure (12) and pressure-correction (13) equations of the SIMPLER iteration more accurately. However, both modifications make the numerical method significantly more expensive.

4.2. *Benchmark Calculations*

In this section the verification of the code is described. Because no analytic solution is available for the general variable viscosity case, the correctness of the numerical solution has been verified by comparing benchmark results that have been published for both 2-D and 3-D convection problems with infinite Prandtl number [39, 40]. Global averaged values like the Nusselt number at the top boundary,

$$Nu = -\frac{1}{l_x l_y} \int \frac{\partial T}{\partial z}(x, y, z = 1)\, dx\, dy,$$

the root-mean-square velocity,

$$v_{\text{rms}} = \left(\frac{1}{l_x l_y} \int (u^2 + v^2 + w^2)\, dx\, dy\, dz \right)^{1/2},$$

and horizontal averaged temperatures,

$$\langle T \rangle_z = \frac{1}{l_x l_y} \int T(x, y, z)\, dx\, dy,$$

with l_x and l_y scaled lengths of the box in x- and y-directions have been calculated. In addition, local values like temperature gradients,

$$q = -\frac{\partial T}{\partial z},$$

and temperature and velocity at specified points have been compared, which indicate more clearly whether local features are accurately resolved.

Benchmark calculations with variable viscosity in 2-D (problems 1 and 2) and in 3-D (problem 3) have been done. Problem 1 corresponds to case 2a in [39]. Stationary convection with temperature-dependent viscosity in a square box is studied. Variable viscosity according to (4b) with $E_4 = \ln(10^3)$ is used. Temperature is fixed to zero at the top and to one at the bottom. Reflecting symmetry is assumed at the sidewalls, zero shear stress at all boundaries. The Rayleigh number is $\text{Ra} = 10{,}000$ based on viscosity $\eta(T = 0)$. A single convection cell develops with thin boundary layers at the top and bottom. The temperature field is shown in Fig. 6. Benchmark results are given in Table 1.

Problem 2 is a modification of this benchmark case with much larger viscosity contrast. All boundary conditions and model parameters are the same, except $\text{Ra} = 0.3$ and

TABLE I
Benchmark Results for Problem 1

	Grid	Nu	v_{rms}	q_1	q_2	q_3	q_4
Benchmark	—	10.0660	480.4334	17.5314	1.0085	26.8085	0.4974
I	32 × 32	10.9823	434.1955	22.5323	0.8369	21.4052	1.3240
	48 × 48	10.4675	467.0277	19.4143	0.9321	24.0071	0.7891
	64 × 64	10.2907	475.2379	18.5086	0.9664	25.4672	0.6321
	96 × 96	10.1683	479.2123	17.9482	0.9902	26.5126	0.5400
	Extrapol.	10.0761	480.2397	17.5849	1.0076	27.1441	0.4909
II	32 × 32	10.6340	446.3899	21.8312	1.0591	20.8398	4.1433
	48 × 48	10.2298	468.2643	18.9488	1.0245	23.7434	2.3037
	64 × 64	10.1331	473.6656	18.2383	1.0151	25.1229	1.4430
	96 × 96	10.0855	477.2843	17.8193	1.0099	26.1127	0.8739
	Extrapol.	10.0690	480.6073	17.5297	1.0074	26.7742	0.5835
III	32 × 32	10.9346	437.1142	22.1751	0.8583	21.2425	1.3496
	48 × 48	10.5298	467.8947	19.7232	0.9368	24.1876	0.7965
	64 × 64	10.3391	475.8778	18.7354	0.9687	25.7341	0.6344
	96 × 96	10.1935	479.5787	18.0605	0.9912	26.7861	0.5405
	Extrapol.	10.0788	479.9999	17.6252	1.0070	27.3365	0.4928
IV	16 × 16	10.2540	465.3548	18.3486	0.9691	25.4857	0.6315
	24 × 24	10.1531	474.7340	17.9082	0.9869	26.5948	0.5441
	32 × 32	10.1187	477.5832	17.7531	0.9949	26.8368	0.5187
	48 × 48	10.0915	479.2310	17.6357	1.0015	26.8936	0.5047
	Extrapol.	10.0647	480.0172	17.5302	1.0077	26.7858	0.4990

Note. Temperature gradients q_1–q_4 have been calculated at $(x, z) = (0, 1), (1, 1), (1, 0)$, and $(0, 0)$. I, uniform grid using bilinear interpolation for viscosity at cell edges and Fromm scheme for advection; II, same as I, except using power-law scheme for advection; III, same as I, except using harmonic interpolation for viscosity; IV, same as I, except using nonequal distribution of grid cells. Given numbers of grid cells belong to the finest global grid. Two refinement levels have been added. The first covers the region $\{(x, z): x \le 0.25 \vee x \ge 0.75 \vee z \le 0.25 \vee z \ge 0.75\}$. The second covers the region $\{(x, z): x \le 0.125 \vee x \ge 0.875 \vee z \le 0.125 \vee z \ge 0.875\}$. The total number of grid cells are 2176, 4896, 8704, and 19584.

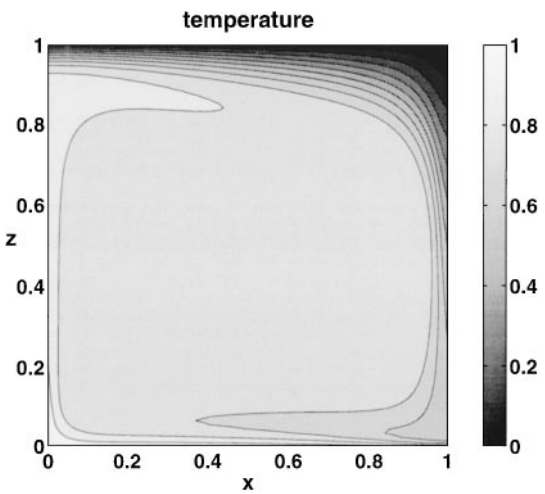

FIG. 6. Stationary 2-D convection with variable viscosity (problem 1).

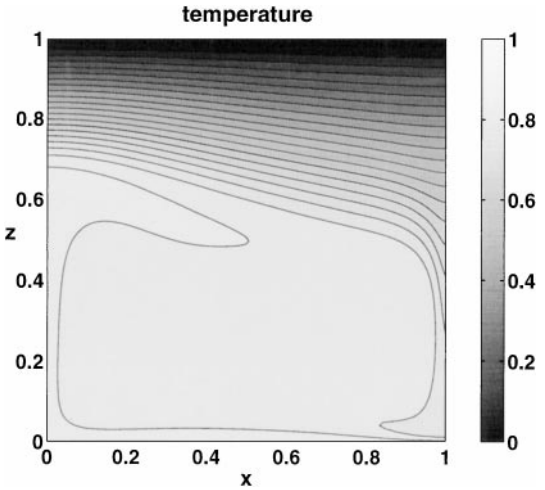

FIG. 7. Stationary 2-D convection with extremely variable viscosity (problem 2).

$E_4 = \ln(10^8)$. Because of the strong temperature-dependence of viscosity a highly viscous stagnant lid develops at the top boundary. Results can be found in Fig. 7 and Table II.

Problem 3 is equivalent to case 2 in [40]. Stationary square-cell convection in Cartesian geometry is studied with plume-like up- and downwellings. Viscosity depends moderately on temperature according to (4a) with $A = \exp(-E_1/(0.5 + E_3))$, $E_1 = 225/\ln(\Delta\eta)$-$0.25\ln(\Delta\eta)$, $E_2 = 0$, $E_3 = 15/\ln(\Delta\eta)$-0.5, and a maximum viscosity contrast $\Delta\eta = 20$. Temperature is fixed to zero at the top and to one at the bottom. Both boundaries are rigid. Reflecting symmetry is assumed at all sidewalls. The Rayleigh number is $\mathrm{Ra} = 20{,}000$ based on viscosity $\eta(T = 0.5)$. Two isosurfaces of temperature are shown in Fig. 8. Benchmark results are given in Table III.

Solutions have been obtained on successively refined grids, allowing extrapolation of results. All extrapolated values are close to the published benchmark results. Because of

TABLE II
Benchmark Results for Problem 2

	Grid	Nu	v_{rms}	q_1	q_2	q_3	q_4
I	32×32	2.3076	246.2311	2.8278	1.8470	5.5275	0.2576
	48×48	2.4041	261.6192	2.9859	1.8974	6.9135	0.2403
	64×64	2.4377	266.3594	3.0388	1.9147	7.5930	0.1986
	96×96	2.4603	268.7643	3.0737	1.9261	8.0841	0.1727
	Extrapol.	2.4759	269.1685	3.0974	1.9336	8.4133	0.1592
III	32×32	2.5113	256.3763	3.2438	1.9017	5.9361	0.3932
	48×48	2.5088	267.4990	3.1986	1.9255	7.1679	0.2506
	64×64	2.4993	269.9527	3.1632	1.9314	7.7753	0.2030
	96×96	2.4885	270.4448	3.1303	1.9339	8.1981	0.1743
	Extrapol.	2.4759	269.1178	3.0977	1.9337	8.4493	0.1600

Note. Temperature gradients q_1–q_4 have been calculated at $(x, z) = (0, 1)$, (1,1), (1, 0), and (0, 0). I, uniform grid using bilinear interpolation for viscosity at cell edges and Fromm scheme for advection; III, same as I, except using harmonic interpolation for viscosity.

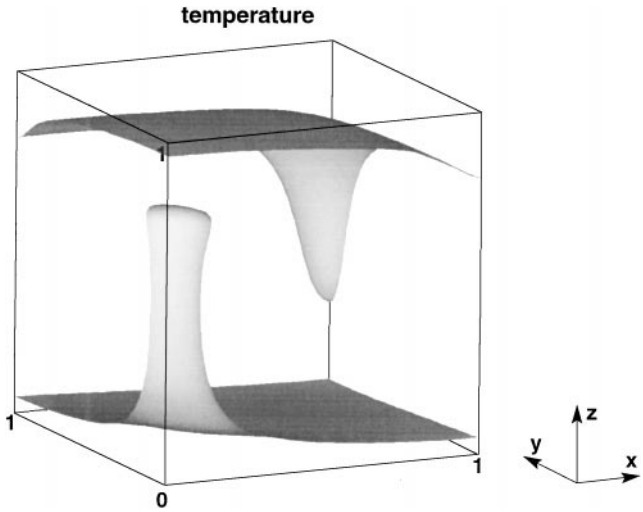

FIG. 8. Stationary 3-D convection with variable viscosity (problem 3). Two temperature isosurfaces ($T = 0.85$ and $T = 0.3$) are shown.

smaller viscosity variations in problem 3 fewer grid points are needed to get accurate results than for problems 1 and 2.

Problem 1 has been solved using Fromm scheme (9) and power-law scheme (10) for advection. Both upwind schemes lead to solutions with similar accuracy. Only the heat flux at the lower left corner is less accurate if the power-law scheme is used (Table I). Bilinear and harmonic interpolation for viscosity at cell edges have been compared in problems 1 and 2. No significant differences can be observed in problem 1 (Table I). Only if viscosity varies more strongly harmonic interpolation becomes more accurate than bilinear interpolation (Table II). The local mesh refinement technique has been verified in problems 1 and 3. In

TABLE III
Benchmark Results for Problem 3

	Grid	Nu	v_{rms}	$\langle T\rangle_{0.5}$	$\langle T\rangle_{0.75}$	T_{P}	w_{P}
Benchmark	—	3.0393	35.13	0.5816	0.5659	0.9053	165.9
I	$16 \times 16 \times 16$	3.0849	35.9987	0.6047	0.5787	0.9199	168.5796
	$24 \times 24 \times 24$	3.0648	35.5494	0.5925	0.5722	0.9129	167.6117
	$32 \times 32 \times 32$	3.0548	35.3692	0.5878	0.5696	0.9098	166.9876
	$48 \times 48 \times 48$	3.0466	35.2341	0.5844	0.5676	0.9074	166.4375
	Extrapol.	3.0393	35.1233	0.5818	0.5659	0.9054	165.9184
IV	$12 \times 12 \times 12$	3.0566	35.5856	0.5992	0.5674	0.9157	165.2988
	$18 \times 18 \times 18$	3.0462	35.3058	0.5898	0.5839	0.9105	165.5992
	$24 \times 24 \times 24$	3.0424	35.2185	0.5864	0.5662	0.9084	165.6593
	$36 \times 36 \times 36$	3.0397	35.1610	0.5839	0.5660	0.9069	165.7218
	Extrapol.	3.0376	35.1197	0.5818	0.5659	0.9058	165.8242

Note. Temperature T_{P} and vertical velocity w_{P} have been taken from $(x, y, z) = (0, 0, 0.5)$. I, uniform grid using bilinear interpolation for viscosity at cell edges and Fromm scheme for advection; IV, same as I, except using nonequal distribution of grid cells. Given numbers of grid cells belong to the finest global grid. One refinement level has been added covering the region $\{(x, y, z)\colon (x \le 1/3 \wedge y \le 1/3) \vee (x \ge 2/3 \wedge y \ge 2/3) \vee z \le 1/6 \vee z \ge 5/6\}$. The total number of grid cells are 7552, 25488, 60416, and 203904.

problem 1 a nonuniform grid with a factor of 4 smaller grid spacing near the boundaries has been used. In problem 3 the grid spacing has been decreased by a factor of 2 in the top and bottom boundary layers and in the up- and downwelling corners (see Tables I and III for a detailed description of the grid structures). Using local mesh refinements leads to more accurate results compared to calculations in which the same total number of grid cells are equally spaced. The improvement of accuracy by increasing the resolution in the critical regions is comparable to the improvement by increasing the resolution everywhere (Tables I and III).

4.3. *Convection Problems with Large Viscosity Gradients*

In geodynamical modeling viscosity gradients which are much larger than in published benchmarks are important. Even in problem 2 viscosity varies only moderately in the interior of the convection cell because most of the viscosity contrast is covered by the stagnant lid. In this section the accuracy of various numerical methods for convection problems with large local gradients in all variables is examined. The numerical solution of the finite-volume multigrid method presented here is compared with numerical solutions obtained by a third order convergent finite-element method [41] and by a hybrid method using finite differences in vertical direction and a spectral formulation in horizontal direction [42].

The test problem is motivated by studies of the interaction of thermal plumes in Earth's mantle with a spreading oceanic ridge [43–45]. Thermal plumes have been proposed to transport hot material from deep in Earth's mantle to the base of the lithosphere. At ridges the plume material may rise up to even shallower depths because the lithosphere is thinned by the diverging plate motion. Studies of plume–ridge interaction are numerically very demanding because in the corner-flow region of the ridge the viscosity gradients become extremely large. The problem is intrinsically 3-D but because only a 2-D version is available for the high-order finite-element code, I restrict the problem to 2-D where the cylindrical plume is replaced by a sheet-like upwelling below the ridge.

Calculations have been done in a box with open bottom and right boundaries. Boundary conditions are defined by

$$\frac{\partial T}{\partial x} = u = \sigma_{xz} = 0 \qquad \text{at } x = 0,$$

$$\left.\begin{aligned} &\frac{\partial T}{\partial x} = w = 0, \quad \frac{\partial \sigma_{xx}}{\partial z} = \rho g \\ \text{or } &\frac{\partial T}{\partial x} = 0, \quad u = u_{\text{shear}}, \quad \frac{\partial w}{\partial x} = 0 \end{aligned}\right\} \qquad \text{at } x = l_x,$$

$$T = 1 + \Delta T_{\text{P}} \exp\left(-\left(\frac{x}{\Delta x_{\text{P}}}\right)^2\right), \quad u = \frac{\partial \sigma_{zz}}{\partial x} = 0 \qquad \text{at } z = 0,$$

$$T = 0, \quad u = u_0 \tanh\left(\frac{x}{x_{\text{R}}}\right), \quad w = 0 \qquad \text{at } z = 1,$$

with σ_{xx}, σ_{xz}, and σ_{zz} stress components. The shear-flow profile $u_{\text{shear}}(z)$ is calculated by

$$\frac{\text{d}}{\text{d}z}\left(\bar{\eta}\frac{\text{d}}{\text{d}z}u_{\text{shear}}\right) = 0,$$

with $u_{\text{shear}}(0) = 0$, $u_{\text{shear}}(1) = u_0$, and $\bar{\eta}(z)$ horizontal averaged viscosity. At $x = l_x$ two

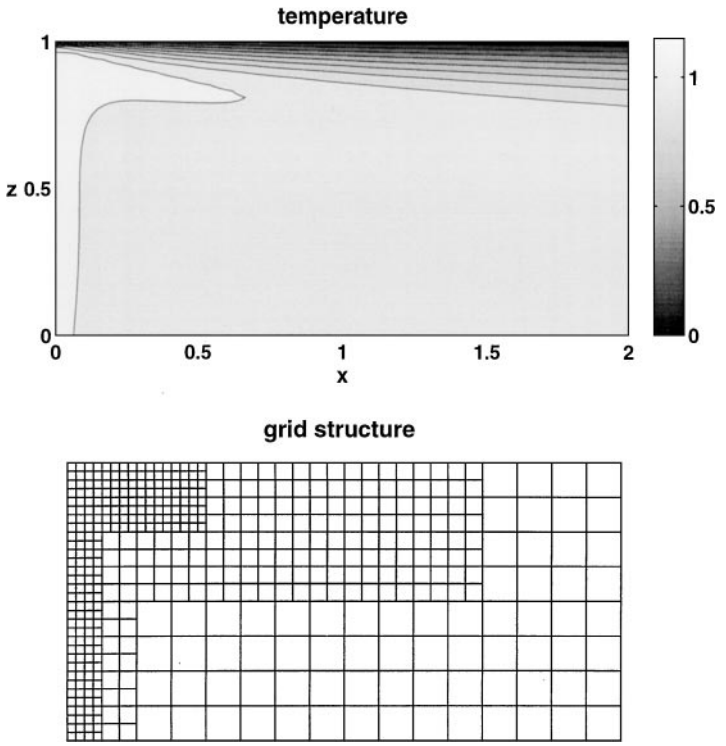

FIG. 9. Stationary plume–ridge interaction with large local viscosity gradients (problem 4). Solution has been obtained by the finite-volume multigrid method using the given nonuniform grid structure with four times more grid cells than are shown, yielding grid spacing $\Delta x = \Delta z = 1/64$ in the corner-flow region of the ridge and in the hot upwelling and $\Delta x = \Delta z = 1/16$ far away from the ridge. Only the left half of the model domain is shown.

different boundary conditions have been applied. The first one has been used in the finite-volume multigrid method and in the finite-element method and the second one in the spectral method. Model parameters are $\mathrm{Ra} = 40{,}000$ based on viscosity $\eta(T = 1, z = 0)$, $\Delta T_\mathrm{P} = 0.15$, $\Delta x_\mathrm{P} = 0.06$, $u_0 = 200$, $x_\mathrm{R} = 0.05$, and $l_x = 4$, except $l_x = 2$ in the spectral method.

Problem 4 is defined by a temperature- and depth-dependent viscosity according to (4a) with $A = \exp(-(E_1 + E_2)/(1 + E_3))$, $E_1 = 18.504$, $E_2 = 4.884$, and $E_3 = 0.21$. Viscosity is limited to a maximum value of 100, yielding lateral viscosity variations of four orders of magnitude within a small region near the ridge. Problem 5 is a modification of problem 4 with even larger viscosity gradients. All model parameters are the same, except $E_1 = 46.261$, yielding lateral viscosity variations of five orders of magnitude.

The stationary solution of problem 4 is shown in Fig. 9. Velocity profiles obtained by the different numerical methods are presented in Fig. 10. The finite-volume multigrid method and the finite-element method produce nearly similar results. Convergence tests have revealed that these solutions are close to the correct result. Both solutions have been obtained on nonuniform grids with smaller grid spacing near the upper left corner. The structure of the nonuniform grid used in the finite-volume multigrid method is shown in Fig. 9. Mesh refinements with a factor of 4 smaller grid spacing have been introduced in the corner-flow region of the ridge and in the hot upwelling. In the finite-element method the grid spacing is nonequal in horizontal and vertical directions. Both grids contain approximately

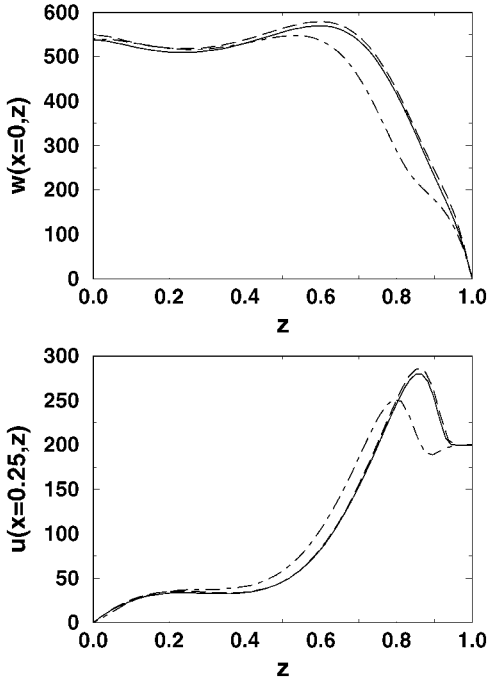

FIG. 10. Vertical velocity at $x = 0$ (top) and horizontal velocity at $x = 0.25$ (bottom) for problem 4 calculated by the finite-element method using 39×48 nonequally spaced grid points (dashed), by the spectral method using 96×48 equally spaced grid points (dot-dashed) and by the finite-volume multigrid method using 2368 nonequally spaced grid cells on the grid shown in Fig. 9 (solid).

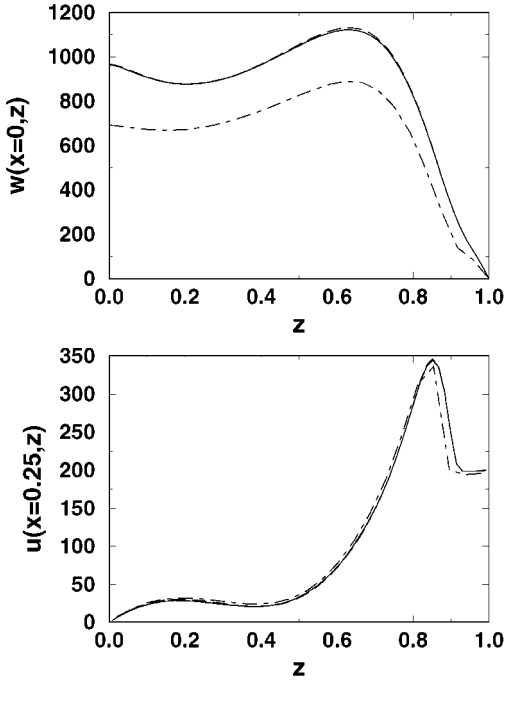

FIG. 11. Vertical velocity at $x = 0$ (top) and horizontal velocity at $x = 0.25$ (bottom) for problem 5 calculated by the finite-volume multigrid method using 256×64 grid cells (dashed) and 96×24 grid cells (dot-dashed) on uniform grids and 2368 nonequally spaced grid cells on the grid shown in Fig. 9 (solid).

the same total number of grid points. Because of the higher convergence order the finite-element method is slightly more accurate than the finite-volume multigrid method. On the other hand, the finite-volume multigrid method is approximately three times faster than the finite-element method for this test problem (3.5 s compared to 9.2 s for 10 time steps on an IBM RS/6000 58H workstation).

The solution of the spectral method differs strongly. A modified boundary condition at the open right boundary has been used in order to apply the fast Fourier transformation. I have varied the aspect ratio of the box and the boundary condition at the right boundary in the finite-volume multigrid method. It turned out that the solution in the corner-flow region of the ridge is not influenced by the boundary condition. Therefore, the differences between the solution of the spectral method and the other solutions cannot be explained by different boundary conditions. It seems that the spectral method overestimates the viscosity in regions with large lateral viscosity variations. Increasing the grid resolution does not lead to a significant improvement of the solution. Accurate results can be obtained by the spectral method only if lateral viscosity variations are significantly reduced.

The accuracy of the finite-volume multigrid method has also been determined for problem 5. Results on locally refined grids and on uniform grids are shown in Fig. 11. Large numbers of grid cells have to be used on uniform grids in order to achieve good resolution. Results on locally refined grids with fewer numbers of grid cells are nearly as accurate. If the same number of grid cells are used on uniform and on nonuniform grids results on nonuniform grids are significantly more accurate.

5. CONCLUSIONS

A finite-volume multigrid method for solving convection problems with variable viscosity in 2-D and 3-D has been presented. The stability of the multigrid method for large viscosity variations has been improved by using more complex multigrid cycles instead of the most simple V cycle. The multigrid method becomes more stable if the number of smoothing iterations on coarser grids is increased. Global viscosity variations of 10^{10} have been considered.

A local mesh refinement technique has been presented which is more efficient and flexible than previously used refinement methods. The nonuniform grid consists of uniform subgrids. This method has been tested for various convection problems. Local mesh refinements can improve the accuracy to a comparable amount as a global refinement of the grid. The formulation of the algorithm allows a simple implementation of complex grid structures. It enables one to introduce new mesh refinements or remove existing ones during calculation. Therefore, it offers a simple possibility of adaptive grid refinements.

The accuracies of different numerical methods have been compared for a test problem with large local viscosity gradients. Numerical methods based on a spectral approach are often used for solving 3-D convection problems. However, it has turned out that spectral methods lead to inaccurate results if the viscosity varies strongly. Therefore, they are not suitable for geodynamical modeling with large viscosity variations. On the other hand, the accuracy of the finite-volume multigrid method is comparable to the accuracy of a third-order convergent finite-element method. The suitability of the finite-volume multigrid method for solving convection problems with strongly variable viscosity has been shown.

ACKNOWLEDGMENTS

I thank U. Christensen, H. Harder, and C. Auth for helpful discussions and three anonymous reviewers for useful comments which helped to improve the manuscript. U. Christensen has done the calculations with the finite-element method and the spectral method. This work was supported by the *Deutsche Forschungsgemeinschaft*.

REFERENCES

1. D. L. Turcotte and G. Schubert, *Geodynamics*, (Wiley, New York, 1982).
2. J. Weertman, The creep strength of the Earth's mantle, *Rev. Geophys. Space Phys.* **8**, 145 (1970).
3. A. Brandt, Multi-level adaptive solution to boundary-value problems, *Math. Comp.* **31**, 333 (1977).
4. A. Brandt and N. Dinar, Multigrid solutions to elliptic flow problems, in *Numerical Methods for Partial Differential Equations*, edited by S. V. Parter (Academic Press, San Diego), 1979, p. 53.
5. W. Hackbusch, *Multi-grid Methods and Applications*, Springer, Berlin (1985).
6. P. Wesseling, *An Introduction to Multigrid Methods* (Wiley, New York, 1992).
7. S. P. Vanka, Block-implicit multigrid solution of the Navier–Stokes equations in primitive variables, *J. Comput. Phys.* **65**, 138 (1986).
8. G. Wittum, Multi-grid methods for Stokes and Navier–Stokes equations, *Numer. Math.* **54**, 543 (1989).
9. B. Koren, Multigrid and defect correction for the steady Navier–Stokes equations, *J. Comput. Phys.* **87**, 25 (1990).
10. S. Zeng and P. Wesseling, Multigrid solution of the incompressible Navier–Stokes equations in general coordinates, *SIAM J. Numer. Anal.* **31**, 1764 (1994).
11. E. M. Parmentier, C. Sotin, and B. J. Travis, Turbulent 3-D thermal convection in an infinite Prandtl number volumetrically heated fluid: Implications for mantle dynamics, *Geophys. J. Int.* **116**, 241 (1994).
12. J. R. Baumgardner, Three-dimensional treatment of convective flow in the Earth's mantle, *J. Stat. Phys.* **39**, 501 (1985).
13. H.-P. Bunge, M. A. Richards, and J. R. Baumgardner, Effect of depth-dependent viscosity on the planform of mantle convection, *Nature* **379**, 436 (1996).
14. H.-P. Bunge, M. A. Richards, and J.R. Baumgardner, A sensitivity study of three-dimensional spherical mantle convection at 10^8 Rayleigh number: Effects of depth-dependent viscosity, heating mode, and an endothermic phase change, *J. Geophys. Res.* **102**, 11991 (1997).
15. A. T. Hsui, W. S. Yang, and J. R. Baumgardner, A preliminary study of the effects of some flow parameters in the generation of poloidal and toroidal energies within a 3-D spherical thermal convection system with variable viscosity, *Pure Appl. Geophys.* **145**, 487 (1995).
16. L. N. Moresi and V. S. Solomatov, Numerical investigation of 2D convection with extremely large viscosity variations, *Phys. Fluids* **7**, 2154 (1995).
17. L. N. Moresi and M. Gurnis, Constraints on the lateral strength of slabs from 3-dimensional dynamic flow models, *Earth Planet. Sci. Lett.* **138**, 15 (1996).
18. L. N. Moresi and A. Lenardic, 3-dimensional numerical simulations of crustal deformation and subcontinental mantle convection, *Earth Planet. Sci. Lett.* **150**, 233 (1997).
19. P. J. Tackley, *Three-dimensional models of mantle convection: Influence of phase transitions and temperature-dependent viscosity*, Ph.D. thesis, California Institute of Technology, Pasadena, 1994.
20. P. J. Tackley, Effects of strongly variable viscosity on three-dimensional compressible convection in planetary mantles, *J. Geophys. Res.* **101**, 3311 (1996).
21. J. T. Ratcliff, P. J. Tackley, G. Schubert, and A. Zebib, Transitions in thermal convection with strongly variable viscosity, *Phys. Earth Planet. Inter.* **102**, 201 (1997).
22. W. B. Moore, G. Schubert, and P. Tackley, Three-dimensional simulations of plume–lithosphere interaction at the Hawaiian swell, *Science* **279**, 1008 (1998).
23. P. J. Tackley, Self-consistent generation of tectonic plates in three-dimensional mantle convection, *Earth Planet. Sci. Lett.* **157**, 9 (1998).

24. R. A. Trompert and U. Hansen, The application of a finite volume multigrid method to 3D flow problems in a highly viscous fluid with variable viscosity, *Geophys. Astrophys. Fluid Dyn.* **83**, 261 (1996).
25. C. Auth and H. Harder, Multigrid solution of convection problems with strongly variable viscosity, *Geophys. J. Int.* **137**, 793 (1999).
26. F. H. Harlow and J. E. Welch, Numerical calculation of time-dependent viscous incompressible flow of fluid with free-surface, *Phys. Fluid* **8**, 2182 (1965).
27. M. Ogawa, G. Schubert, and A. Zebib, Numerical simulations of three-dimensional thermal convection in a fluid with strongly temperature-dependent viscosity, *J. Fluid Mech.* **233**, 299 (1991).
28. S. V. Patankar, *Numerical Heat Transfer and Fluid Flow* (McGraw-Hill, New York, 1980).
29. A. Brandt, Multilevel computations: Review and recent developments in *Multigrid Methods: Theory, Applications and Supercomputing*, edited by S. F. McCormick (Dekker, New York, 1988). p. 35.
30. P. Wesseling, Cell-centered multigrid for interface problems, *J. Comput. Phys.* **79**, 85 (1988).
31. R. A. Trompert and U. Hansen, On the Rayleigh number dependence of convection with a strongly temperature-dependent viscosity, *Phys. Fluids* **10**, 351 (1998).
32. J.-A. Désidéri and P. W. Hemker, Convergence analysis of the defect-correction iteration for hyperbolic problems, *SIAM J. Sci. Comput.* **16**, 88 (1995).
33. P. W. Hemker, On the order of prolongations and restrictions in multigrid procedures, *J. Comput. Appl. Math.* **32**, 423 (1990).
34. M. Khalil and P. Wesseling, Vertex-centered and cell-centered multigrid for interface problems, *J. Comput. Phys.* **98**, 1 (1992).
35. R. E. Alcouffe, A. Brandt, J. E. Dendy, and J. W. Painter, The multi-grid method for diffusion equation with strongly discontinous coefficients, *SIAM J. Sci. Comput.* **2**, 430 (1981).
36. J. E. Dendy, Black box multigrid, *J. Comput. Phys.* **48**, 366 (1982).
37. J. E. Dendy, Two multigrid methods for three-dimensional problems with discontinous and anisotropic coefficients, *SIAM J. Sci. Statist. Comput.* **8**, 673 (1987).
38. D. Bai and A. Brandt, Local mesh refinement multilevel techniques, *SIAM J. Sci. Statist. Comput.* **8**, 109 (1987).
39. B. Blankenbach, F. Busse, U. Christensen, L. Cserepes, D. Gunkel, U. Hansen, H. Harder, G. Jarvis, M. Koch, G. Marquart, D. Moore, P. Olson, H. Schmeling, and T. Schnaubelt, A benchmark comparison for mantle convection codes, *Geophys. J. Int.* **98**, 23 (1989).
40. F. H. Busse, U. Christensen, R. Clever, L. Cserepes, C. Gable, E. Giannandrea, L. Guillou, G. Houseman, H.-C. Nataf, M. Ogawa, M. Parmentier, C. Sotin, and B. Travis, 3D convection at infinite Prandtl number in Cartesian geometry—A benchmark comparison, *Geophys. Astrophys. Fluid Dyn.* **75**, 39 (1993).
41. U. R. Christensen, An Eulerian technique for thermomechanical modeling of lithospheric extension, *J. Geophys. Res.* **97**, 2015 (1992).
42. U. R. Christensen and H. Harder, 3-D convection with variable viscosity, *Geophys. J. Int.* **104**, 213 (1991).
43. N. M. Ribe, U. R. Christensen, and J. Theißing, The dynamics of plume-ridge interaction. 1. Ridge-centered plumes, *Earth Planet. Sci. Lett.* **134**, 155 (1995).
44. G. Ito, J. Lin, and C. W. Gable, Dynamics of mantle flow and melting at a ridge-centered hotspot: Iceland and the Mid-Atlantic Ridge, *Earth Planet. Sci. Lett.* **144**, 53 (1996).
45. G. Ito, Y. Shen, G. Hirth, and C. J. Wolfe, Mantle flow, melting, and dehydration of the Iceland mantle plume, *Earth Planet. Sci. Lett.* **165**, 81 (1999).